scientific reports

Check for updates

OPEN

Efficient crystal structure materials as reactive sorbent for the CO_2 and CH_4 adsorption and storage

R. Essehli[1], B. Aïssa[2], T. Altamash[2,3], M. Lachkar[4], M. Atilhan[5], B. El Bali[6], G. R. Berdiyorov[2] & A. Amhamed[2]✉

The efficient dirubidium cobalt bis(dihydrogendiphosphate) dihydrate compound is successfully synthesized in a solution and used as a reactive sorbent for the CO_2 and CH_4 gases adsorption and storage. A crystal of this $Rb_2Co(H_2P_2O_7)_2{\cdot}2H_2O$ compound has been isolated and characterized by single X-ray diffraction analysis and was found to crystallize in the triclinic system ($P\bar{1}$) with the cell parameters (Å): 6.980(1), 7.370(1), 7.816(1), 81.74(1), 70.35(1), 86.34(1); V = 374.68(9) Å3, Z = 2. The crystal-packing consists of a three-dimensional framework made upon corners and edges sharing of [RbO_7], [$H_2P_2O_7$] and [CoO_6] entities, furthermore linked by a network of H-bonds. The UV–Vis spectroscopy revealed usual transitions between the ground state 4T1g and the upper levels 4T2g, 4A2g and 4T1g (P). Moreover, the CO_2 and CH_4 gases sorption measurements were successfully performed at two different temperatures (25 and 45 °C) and various pressures ranging from vacuum to 50 bar. Our results show that rate of CO_2 and CH_4 capturing was 3.10 mmol/g and 2.35 mmol/g at temperature 25 °C and pressure 50 bar, respectively. This compound showed a clear potential for CO_2/CH_4 adsorption and storage thereby paving the way towards its exploration and adaptation for capturing and collecting carbon dioxide and greenhouse gases from the air, and their conversion into hydrocarbon fuels using existing mature technologies. We have also conducted density functional theory calculations to study the CO_2 and CH_4 adsorption properties of $Rb_2Co(H_2P_2O_7)_2{\cdot}2H_2O$. The simulation results show enhanced adsorption of both types of molecules on the surface of the material.

Climate change is a critical world pressing challenge. Emission of greenhouse gases, including nitrous oxide (N_2O), methane (CH_4) and carbon dioxide (CO_2), have increased global temperatures by around 1 °C since pre-industrial times, where CO_2 alone is contributing to more than 60% of this global warming[1–3]. The increasing percentage of CO_2 and CH_4 gases into the atmosphere is considered nowadays as a serious threat as it has a range of potential ecological, physical and health impacts, including extreme weather events (such as floods, droughts, storms), sea-level rise, altered crop growth, and disrupted water systems. To mitigate climate change, UN member parties have set a target, in the Paris Agreement, of limiting average warming to 2 °C above pre-industrial temperatures.

From technical viewpoint, the absorption and adsorption of greenhouse gases is one of the most challenging technological issues for researchers and environmentalist towards developing sustainable technologies based on new materials to control and mitigate the anthropogenic emission[1]. For more than six decades, solvent absorption technologies, and particularly aqueous alkanolamines, were the most commonly employed chemical absorbents for CO_2 gas removal.

However, these adsorption processes are associated with various industrial limitations[1,4]. In the recent development in the chemical sciences field, ionic liquids (ILs) have shown some potential features for CO_2 capturing due to their unique chemical and physical properties and replacement capability of serious conventional solvents.

[1]Energy and Transportation Science Division, Oak Ridge National Laboratory (ORNL), 1 Bethel Valley Rd, Oak Ridge, TN 37830, USA. [2]Qatar Environment and Energy Research Institute (QEERI), Hamad Bin Khalifa University (HBKU), Qatar Foundation, P.O. Box 34110, Doha, Qatar. [3]Materials Science, Energy and Nanoengineering Department (MSN), Mohammed VI Polytechnic University (UM6P), Lot 660 – Hay Moulay Rachid, 43150 Ben Guerir, Morocco. [4]University Sidi Mohamed Ben Abdellah, Fez City, Morocco. [5]Department of Chemical and Paper Engineering, Western Michigan University, Floyd Hall, A-230, Kalamazoo, MI 49008, USA. [6]Laboratory of Mineral Solid and Analytical Chemistry, "LMSAC", Department of Chemistry, Faculty of Sciences, University Mohamed I, Po. Box 717, 60000 Oujda, Morocco. ✉email: aamhamed@hbku.edu.qa

In addition, deep eutectic solvents (DESs) have demonstrated many unusual characteristics for CO_2 absorption at room temperature[5–9], including negligible vapor pressure, non-flammability, wide liquid range, high thermal and chemical stabilities and high solvation capacity[10,11]. DES term was introduced by the team of Abbott[9] in 2003 in order to overcome some of the IL's drawbacks. Similarly, dried solid materials are another type rational choice for gas adsorption in separation technologies which helps to minimize the energy consumption and regeneration processes up to some extent. Thus, a number of newer solid materials are now being synthesized and characterized and tuned further in order to enhance their practical applicability for specific gas or gas mixtures[12–15]. Indeed, gas adsorptivity capacity is closely related to accessible surface structure and molecular arrangement of the solid crystal. Typically, the flue gas composition consists of CO_2, H_2O, CO, N_2, H_2S, H_2, Ar, NO_x, SO_x, Hg and Cd[16]. In some cases, CH_4 slip into flue gas stream could occur when the incomplete exothermic oxidation of a fuel took place due to insufficient amount of oxygen to the combustion system. R&D tends to focus on safe and eco-friendly porous organic and inorganic materials for their use in gas storage[17–20]. Since then, several inorganic phosphate-based compounds have been extensively studied and were found to not only be able to capture CO_2 and CH_4 but also to act as storage for clean energy. As a contribution to this internationally critical research effort, we successfully designed and synthesized efficient diphosphates, namely dirubidium cobalt bis(dihydrogendiphosphate) dihydrate ($Rb_2Co(H_2P_2O_7)_2{\cdot}2H_2O$), and assessed it as CO_2 and CH_4 gases adsorption and storage. Our results show a rate of CO_2 and CH_4 capturing of 3.10 mmol/g and 2.35 mmol/g at temperature of 25 °C and pressure of 50 bar. Moreover, gas sorption comparison study demonstrated a clear evidence of a selective behavior of our compound for CO_2 and CH_4 gases at each temperature and pressure, and revealed that adsorbtivity of CO_2 is more than that of the CH_4 at different temperatures and pressures, making this diphosphate a promising candidate for greenhouse gases adsorption and storage. First principles density functional theory (DFT) calculations also reveal strong adsorption of both CO_2 and CH_4 molecules on the surface of the $Rb_2Co(H_2P_2O_7)_2{\cdot}2H_2O$ material. The adsorption energy of CO_2 molecules is smaller (i.e., stronger adsorption) as compared to the adsorption energy of CH_4 molecule due to covalent character of bonding of the CO_2 molecule on the surface of the material as revealed in our electronic structure calculations.

The present work focuses on designing a diphosphate that can be used for direct air capture of CO_2 and CH_4 molecules. This work could lead to promising technology to create CO_2 and CH_4 outlet from the earth's atmosphere due to several advantages such as the easy application and geographical independence. The present new configuration can also help bypassing the high cost of DAC systems for greenhouse gas capture.

Methods

Sample fabrication

Single crystals of $Rb_2Co(H_2P_2O_7)_2{\cdot}2H_2O$ was prepared according to the method reported in our previous works[21–26]. $K_4P_2O_7$ (1 mmol), Rb_2CO_3 (1 mmol), and $CoCl_{2.6}H_2O$ (0.5 mmol), dissolved in a few ml of diluted HCl (0.75 mL of HCl 0.1 M), as structure directing agent. The mixture was stirred for 2 h. The evaporation of the solvent water was allowed for one week, at room temperature. Prismatic crystals with edge-length up to 0.2 mm was deposited at the end of this period, then filtered-off and washed with water–ethanol mixture (concentration 20:80).

Characterization

The reported crystallographic data for $Rb_2Co(H_2P_2O_7)_2{\cdot}2H_2O$ are given in Table 1. The $Rb_2Co(H_2P_2O_7)_2{\cdot}2H_2O$ selected crystal shows an excellent structural quality with exceptional low Rint factors. The hydrogen atoms are localized in different Fourier maps. They are also refined independently using solely the condition that the temperature parameters of hydrogen atoms in H_2O molecules and $H_2P_2O_7$ groups are equal. X-ray diffraction data were collected on an Oxford Diffraction XCALIBUR four-circles X-ray diffractometer using graphite monochromatized MoKα radiation (λ = 0.7173 Å) equipped with a SAPPHIR CCD two-dimensional detector. The intensity data were corrected for Lorentz and polarization effects. A numeric analytical absorption correction was carried out with the program CrysAlis RED[27]. The metal and phosphorus atoms were located by direct methods, using the SHELXS-97 program[28], while the remaining atoms were found from successive Fourier difference maps. Atomic positions were refined by full matrix least-squares method using SHELXL-97 program[29]. Full-matrix least squares refinement was based on F2. Thermal displacements of all non-hydrogen atoms were refined anisotropically. Pertinent crystallographic details are given in Tables 1, 2 and 3. Graphics have been performed using DIAMOND program[30]. Tables of crystal structures and refinements, notably full bond lengths and angles, and anisotropic thermal parameters have been deposited with the Inorganic Crystal Structure Database, FIZ, Hermann von Helmholtz Platz 1, 76,344 Eggenstein Leopoldshafen, Germany; fax: (+ 49) 7247 808 132; Email: crysdata@fiz-karlsruhe.de. CSD-deposition numbers are respectively 421807 for $Rb_2Co(H_2P_2O_7)_2{\cdot}2H_2O$.

Gas adsorption/sorption device

The absorption/desorption measurements of carbon dioxide (CO_2) and methane (CH_4) with the synthesized material were successfully performed at temperatures of 298 and 318 K, and from vacuum to 50 bars, by using the specific high pressure "magnetic suspension sorption apparatus (MSA)" equipment, purchased from Rubotherm Präzisionsmesstechnik GmbH. This tool has the ability to raise the pressure up to 350 bars, and temperature up to 373 °K. The pressure transducers (ParoscientificTM, USA) were installed to measure the pressure from vacuum to 350 bars with an accuracy of 0.01% bar, and temperature sensor (Minco PRT, USA) with a sensitivity of ± 0.5 °C. The detailed experimental procedure and calibration are detailed in elsewhere[31–33].

Chemical formula	$Rb_2Co(H_2P_2O_7)_2{\cdot}2H_2O$
Formula weight	387.9 (g/mol)
Colour	Pink
Symmetry (S.G.)	Triclinic (P-1)
Unit cell parameters (Å, °) a/b/c/α/β/γ	6.980(1) 7.370(1) 7.816(1) 81.74(1) 70.35(1) 86.34(1)
V (Å^3)	374.68(9)
Z	2
$\rho_{calc.}$ (g cm^{-3})	2.738
Temperature (K)	302(2)
Diffractometer	Oxford Diffraction CCD
Radiation MoKα, (Å)	0.71069
2θ-range	2.842–27.679
Reciprocal space	$-8 \le h \le 8$ $-8 \le k \le 9$ $-9 \le l \le 9$
Collected reflections	1508
Refined parameters	118
R(F)/wR2(F^2)	0.0340/0.0851

Table 1. Crystal data and structure refinement for $Rb_2Co(H_2P_2O_7)_2{\cdot}2H_2O$.

Atom	*Site*	x	y	z	Ueq
Co1	1c	0.0000	0.5000	0.0000	0.0152 (2)
P1	2i	0.26553 (15)	0.20005 (14)	−0.25549 (14)	0.0153 (2)
P2	2i	−0.14918 (16)	0.26198 (13)	−0.25914 (14)	0.0158 (2)
O1	2i	0.2558 (4)	0.3480 (4)	−0.1401 (4)	0.0231 (7)
O2	2i	0.4544 (4)	0.2162 (4)	−0.4320 (4)	0.0261 (7)
H2	2i	0.563(5)	0.266(6)	−0.420(7)	0.031
O3	2i	0.2445 (5)	0.0076 (4)	−0.1553 (4)	0.0275 (7)
O4	2i	0.0920 (4)	0.2310 (4)	−0.3509 (4)	0.0225 (6)
O5	2i	−0.1883 (4)	0.3833 (4)	−0.1114 (4)	0.0197 (6)
O6	2i	−0.2239 (4)	0.3339 (4)	−0.4151 (4)	0.0220 (6)
O7	2i	−0.2412 (5)	0.0693 (4)	−0.1731 (4)	0.0259 (7)
H7	2i	−0.234(8)	0.039(6)	−0.060(3)	0.031
O8	2i	0.0601 (5)	0.7123 (4)	−0.2196 (4)	0.0262 (7)
H8A	2i	0.104(6)	0.693(6)	−0.331(2)	0.031
H8B	2i	0.126(6)	0.803(4)	−0.213(5)	0.031
Rb1	2i	−0.40751 (7)	0.71568 (6)	−0.21039 (6)	0.03062 (18)

Table 2. Atomic coordinates and isotropic displacement parameters U_{eq}[a] for $Rb_2Co(H_2P_2O_7)_2{\cdot}2H_2O$.

Density functional theory

Computer simulations are conducted using DFT within the generalized gradient approximation of Perdew–Burke–Ernzerhof (PBE) to describe the exchange–correlation energy[34]. The plane-wave basis set with a cut-off energy of 1360.57 eV is used to describe the atoms in the system. The Brillouin zone integration was conducted using $15 \times 15 \times 15$ Monkhorst–Pack k-points sampling[35] for the unit cell structure of the material. The convergence criterion for Hellman–Feynman forces was 0.01 eV/Å. Interactions of CO_2 and CH_4 molecules with the surface of the material is characterized by the electron difference density which is defined as the difference between the self-consistent valence charge density and the superposition of atomic valence densities[36]. Simulations are conducted using the computational package Atomistix toolkit[37,38].

(1)	
Atoms 1,2	**d 1,2* [Å]**
Co1—O5	2.087(3)
Co1—O5^{i}	2.087(3)
Co1—O8	2.097(3)
Co1—O8^{i}	2.097(3)
Co1—O1^{i}	2.103(3)
Co1—O1	2.103(3)
P1—O1	1.496(3)
P1—O3	1.509(3)
P1—O2	1.551(3)
P1—O4	1.612(3)
P2—O6	1.498(3)
P2—O5	1.503(3)
P2—O7	1.559(3)
P2—O4	1.608(3)
Rb1—O2^{iv}	2.892(3)
Rb1—O7^{vii}	3.010(3)
Rb1—O3^{viii}	3.100(3)
Rb1—O5^{iii}	3.127(3)
Rb1—O1^{i}	3.219(3)
Rb1—O4^{iv}	3.377(3)
Rb1—O1^{ix}	3.562

Table 3. Bond lengths (Å) values in the structures of $Rb_2Co(H_2P_2O_7)_2{\cdot}2H_2O$. *Symmetry codesin (1) and (2): (i) − x, 1 − y, − z; (ii) 1 + x, y, z; (iii) − 1 − x, 1 − y, − z; (iv) − x, 1 − y, − 1 − z; (v) 1 + x, − 1 + y, z; (vi) x, − 1 + y, z; (vii) x, 1 + y, z; (viii) − 1 + x, 1 + y, z; (ix) − 1 + x, y, z in (**3**): (i) − x, 1 − y, − z; (ii) − x, 1 − y, − 1 − z; (iii) − 1 − x, 1 − y, − z; (iv) 1 + x, − 1 + y, z; (v) x, − 1 + y, z; (vi) x, 1 + y, z; (vii) 1 − x, y − 1, z.

Results and discussions

Crystal structure study

The structural model in $Rb_2Co(H_2P_2O_7){\cdot}2H_2O$ consists of a 3D framework, made from corners and edges sharing of $[RbO_7]$, $[H_2P_2O_7]$ and $[CoO_6]$ entities. Figure 1a,b depict the shape of the crystal structure of the title compound onto the crystallographic (010) and (001) planes. H-bonds are represented by dashed lines. These figures have been drawn according to the respective atomic coordinates reported in Table 2 and to the bond lengths and angles represented in Table 3. The structure might be described in terms of isolated $[CoO_4(H_2O)_2(H_2P_2O_7)_2]$ units which propagates tri-dimensionally through Rb–O interactions and an intricate H-bonds network between the $H_2P_2O_7$'s hydroxyl groups. Such unit $[CoO_4(H_2O)_2(H_2P_2O_7)_2]$ results from the edge sharing $[CoO_4(H_2O)_2]$ octahedron and $[H_2P_2O_7]$ double tetrahedrons. The unit cell contains two distinctive phosphorous (V) sites coordinated by four (04) oxygen atoms in a slightly distorted tetrahedron. Two (02) tetrahedra share an apex to form the dihydrogenpyrophosphate group $H_2P_2O_7$. Average <P—O> distance is about 1.551 Å. This value is similar to its homologous distances in the known isoformular compounds $(NH)_2Co(H_2P_2O_7)_2{\cdot}2H_2O$[21]. As in the other mixed pyrophosphates, $H_2P_2O_7$ shows almost an eclipsed conformation. The ∠(P–O–P) bridging angle is one feature characterizing the $[H_2P_2O_7]_2$- anion, here of 129.3°. In this new pyrophosphates, Co^{2+} cations are placed on inversion centre position (0, 1/2, O). Their octahedral coordination is composed of four (04) Oxygen atoms from two (02) bidendate $[H_2P_2O_7]$ groups and the remaining two (02) Oxygen from the water molecules. However, the M^{2+} cation in the orthorhombic form of $K_2M(H_2P_2O_7)_2{\cdot}2H_2O$ (M=Co, Ni, Cu)[22] is located in the mirror plane within an octahedral coordination formed by two (02) bidendate $[H_2P_2O_7]_2$- counter ions and two (02) water molecules. Average $\bar{d}$(Co—O) is of 2.095 Å, value was compared with recently the one reported value of $(NH_4)_2Co(H_2P_2O_7)_2{\cdot}2H_2O$ (2.053 Å) (Table 3)[21].

UV–Vis study

The UV–Visible spectrum of the $Rb_2Co(H_2P_2O_7){\cdot}2H_2O$ is displayed in Fig. 2a,b. It might be described in terms of electronic transitions between the ground state 4T1g and the upper ones 4T2g, 4A2g and 4T1g(P). In fact, three spins allowed transitions may be expected. The lowest energy band observed near 7109.6 cm^{-1} is assigned to the 4T2g → 4T1g transition, while the main absorption band in the visible region near 14,581 cm^{-1} is rather assigned to 4T2g (P) → 4T1g.

CO_2 and CH_4 adsorption and desorption

The ultimate aim of the present work is to experimentally investigate the sorption capacity of CO_2 and CH_4 onto the $Rb_2Co(H_2P_2O_7){\cdot}2H_2O$. For both gases, the experiments were performed at temperatures of 298 and 318 K, respectively. At each temperature, cycles of adsorption and desorption were run by stepwise increment/

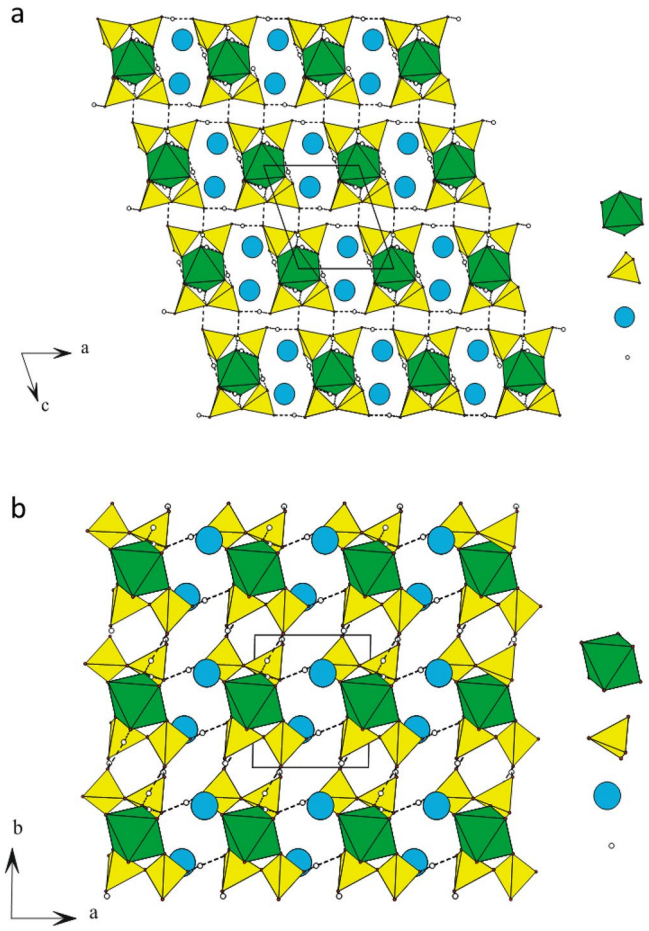

Figure 1. (**a**, **b**) $Rb_2Co(H_2P_2O_7)_2{\cdot}2H_2O$ as representative crystal structure, projections of the framework onto crystallographic (010) and (001) planes. H-bonds are represented as dashed lines.

decrement process of CO_2 and CH_4 pressures, ranging from vacuum to 50 bars and its vice-versa. At each temperature, individual cycles of CO_2 and CH_4 were recorded that consist of 12 adsorption and 8 desorption points with $Rb_2Co(H_2P_2O_7){\cdot}2H_2O$, illustrated in supplementary Tables S1 and S2. Similarly, all the values were used to plot the figures to understand the behavior (hysteresis and physisorption) of $Rb_2Co(H_2P_2O_7){\cdot}2H_2O$ at moderate and higher temperature from vacuum to high pressure through a programmed adsorption–desorption cycle in Figs. S1–S4. On looking over the plots (Figs. S1–S4) of their corresponding gas at both the temperature, figures demonstrate a smooth trend of variation with respect to pressure by overlapping adsorption and desorption points. These collective adsorption–desorption trends indicate that there are no hysteresis, and no significant changes occur in material. Additionally, it has to be mentioned that in order to obtain reliable data, peripheral conditions like humidity, ambient pressure, and temperature were taken care of [39]. The similar trend of variation (adsorption and desorption pressure point that lies at same plotted line) have found in our recently published work with $(NH_4)_2\ Mg(H_2P_2O_7)_2{\cdot}2H_2O$) with CO_2 and CH_4 at 298 and 318 K [40] Figs. S1, S2 and S3 show a common thermodynamic trend of variation; solubility of gas decreases when increasing the temperatures, and increases when increasing the pressures which in turns lead to increase the adsorption capacity of CO_2 and CH_4 in m.mol per gram of sample. Although, similar trend of adsorption/desorption indicates physisorption of gases gives the advantage of reusability for energy and economic saving [41,42] point of view as ionic liquids and deep eutectic solvent being tested as liquid absorbent [33,39,42–44]. Consequently, this efficient crystal could be very useful materials for one of flue gas process treatment stages. Furthermore, the trend of CO_2 and CH_4 adsorption shows that our new crystal could be easily regenerated in an efficient process. A close scrutiny of adsorption results shows that CO_2 (3.1016 m mol/g) sorption is higher than CH_4 (2.3467 m mol/g) at temperature 298 K and at pressure of 50 bars, where maximum sorption was expected. This comparison gives clear evidence of a selective behavior of the crystal acidic pyrophosphate $Rb_2Co(H_2P_2O_7){\cdot}2H_2O$ for CO_2 and CH_4 gases at each temperature and pressure. On further reviewing Figs. 3 and 4 single crystal sample shows that the sorptivity of CO_2 is higher than that of the CH_4 at 318 K temperatures, additionally, ~ 0.5 bar sorptivity difference between both gases at both the temperatures at its highest measured pressure. However, this is the continuation of our recent published research work [40] and comparative plot of present and previously investigated has been included in supporting information as Fig. S5. Previously used material ($(NH_4)_2\ Mg(H_2P_2O_7)_2{\cdot}2H_2O$) for CO_2 and CH_4 at 50 bar, and 298 K and 318 K values shows that adsorb 3.3858 m mol/g, 2.9657 m mol/g of CO_2 of $(NH_4)_2\ Mg(H_2P_2O_7)_2{\cdot}2H_2O$, respectively, at the same pressure and temperatures 5.3234 m mol/g and 8.2909 m mol/g respectively for CH_4. The CO_2

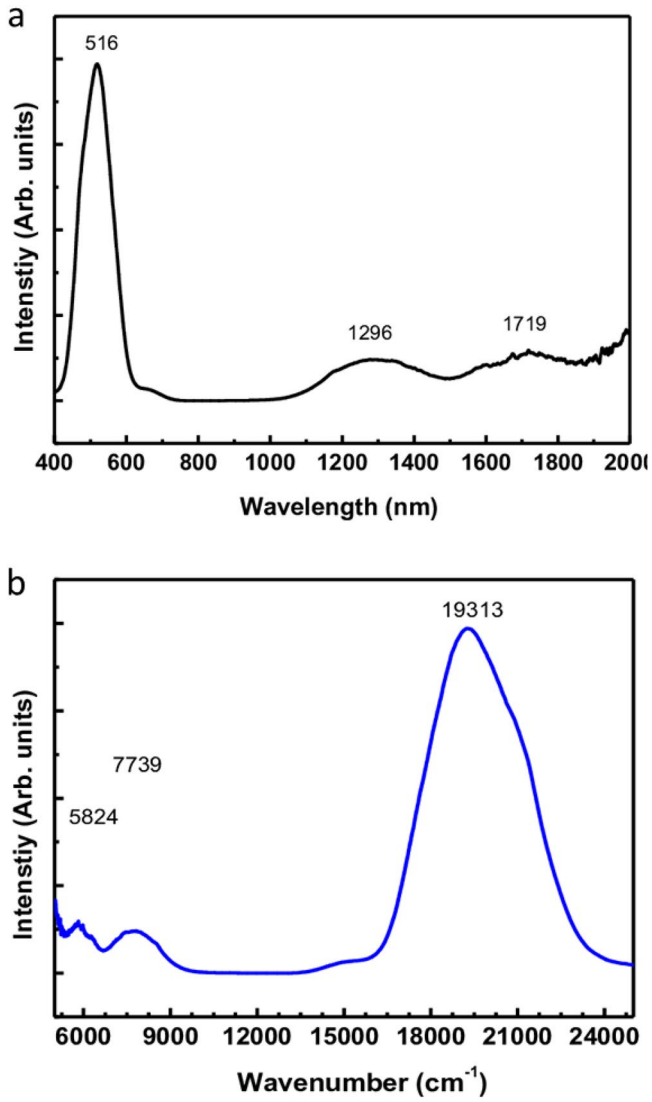

Figure 2. UV–Visible spectra of the $Rb_2Co(H_2P_2O_7)_2{\cdot}2H_2O$ compound.

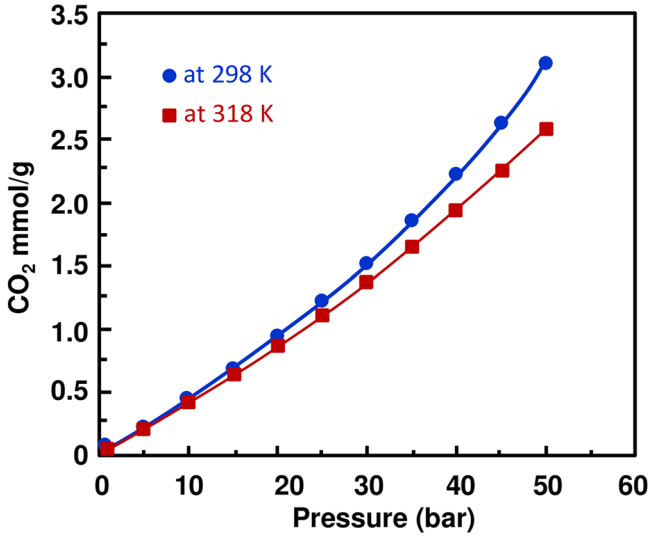

Figure 3. CO_2 absorption trends in $Rb_2Co(H_2P_2O_7)_2{\cdot}2H_2O$ at 298 and 318 K, and different pressures.

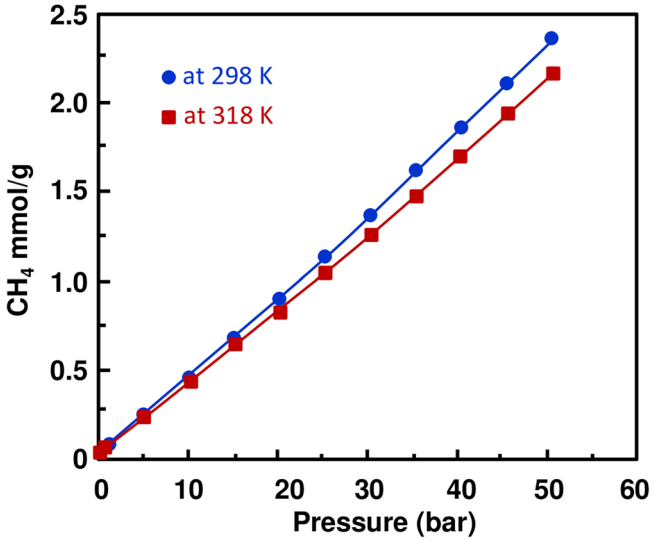

Figure 4. CH_4 absorption trends in $Rb_2Co(H_2P_2O_7)_2{\cdot}2H_2O$ at 298 and 318 K and different pressures.

sorption is almost close to the currently investigated sample however CH_4 sorption values are 3–4 fold higher in comparison with $Rb_2Co(H_2P_2O_7){\cdot}2H_2O$ at temperatures. Moreover, on comparing CO_2 sorption data of this work and hydroxy metal carbonates $M(CO3)_x(OH)_y$ (M=Zn, Zn–Mg, Mg, Mg–Cu, Cu, Ni, and Pb) [45], found that $Rb_2Co(H_2P_2O_7){\cdot}2H_2O$ shows higher values 35 bar at 318 K, although hydroxy metal carbonates were measured at 316 K. The enhanced CO2 sorption capacity of $Rb_2Co(H_2P_2O_7){\cdot}2H_2O$ compared to hydroxy metal carbonates may be attributed to its unique three-dimensional framework. The presence of [RbO7], [H2P2O7], and [CoO6] entities interconnected through a dense network of hydrogen bonds can offer specific adsorption sites and channels, facilitating better gas uptake. Furthermore, the preferential adsorption of CO2 in $Rb_2Co(H_2P_2O_7){\cdot}2H_2O$ over hydroxy metal carbonates can be intricately linked to the electronic nature of its components. The coordination of the Co ion, often known for its variable oxidation state and magnetic properties, combined with the phosphate groups, may provide an electron-rich environment. This can enhance the Lewis acid–base interactions with the electrophilic carbon of CO_2, resulting in better sorption. Additionally, the dense hydrogen-bonding network might create a dynamic environment, allowing for reversible adsorption and facilitating efficient gas uptake and release. In Fig. 5, we have demonstrated the CO_2/CH_4 ideal selectivity results at 298 K and 318 K from pressure 1–50 bar (11 sorption data point). The CO_2/CH_4 (mmol gas per g of sample) ideal selectivity at 298 K was higher as compared to 318 K, as expected, and trends of variations are close to each other at both the temperatures. Furthermore, after 35 bar significantly increased values were noticed, and difference was reached at maximum investigated pressure. Last but not the least, CO_2/CH_4 ideal selectivity of $Rb_2Co(H_2P_2O_7){\cdot}2H_2O$ is much higher than $(NH_4)_2Mg(H_2P_2O_7)_2{\cdot}2H_2O$ of previous work [40] at all the pressures and temperatures. CO_2, with its linear

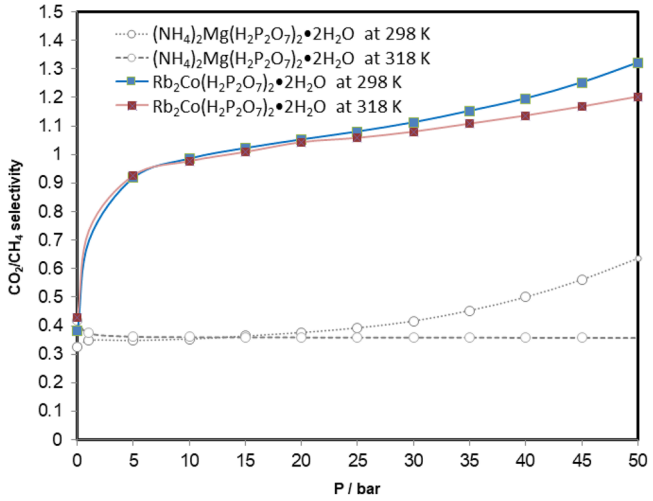

Figure 5. CH_4/CO_2 ideal selectivity at low and high pressures for studied $Rb_2Co(H_2P_2O_7)_2{\cdot}2H_2O$ at 298 and 318 K and different pressures.

molecular geometry and inherent quadrupole moment, interacts differently with adsorbents compared to tetrahedral CH_4. $Rb_2Co(H_2P_2O_7)\cdot 2H_2O$ might provide specific sites where the CO2 quadrupole can align favorably, leading to enhanced selectivity. Rb's relatively larger ionic size may influence the pore geometries and accessibility, leading to differential interactions with CO_2 and CH_4 molecules, thus affecting the separation efficiency. Furthermore, due to these large ionic radii for Rb and diffuse electron cloud can also lead to induction of more significant dispersion forces. This, combined with the potential electronic interactions from Co and phosphate entities, might selectively favor the adsorption of CO2 over CH4, fine-tuning the separation efficiency.

Simulation results for CO_2 and CH_4 adsorption

We started by creating and optimizing the unit cell structure of the $Rb_2Co(H_2P_2O_7)\cdot 2H_2O$ material using our experimental findings. Figure 6 shows the unit cell structure of the material after geometry optimization. The optimized structure has a triclinic lattice with parameters a = 7.008 Å, b = 7.44 Å, and c = 7.71 Å, and angles α = 82.24, β = 72.44 and γ = 86.42. Using this unit cell structure, we have constructed and further optimized 21 slab geometries with 5 different surface symmetries (100, 001, 010, 101, 011, 110, and 111) and 3 different terminations (P-, Ru-, and Co-terminations). Total energy calculations[46,47] show that a slab with Co-terminated 111 surface has the lowest energy for this material. Next, we study the adsorption of CO_2 and CH_4 molecules on this surface. To characterize the adsorption properties of the material, we have conducted total energy and electron localization function calculations. The adsorption energies are calculated as:

$$E_{ads} = E_{(slab+mol)} - E_{slab} - E_{mol},$$

where E_{mol} is the total energy of the isolated molecule and E_{slab} is the total energy of the slab in the absence of the molecule.

To find the adsorption sites with minimum energy, we have started our calculations for 15 different locations and orientations of the molecules on Co-terminated 111 surface of $Rb_2Co(H_2P_2O_7)\cdot 2H_2O$. The atoms at bottom layer of the slab kept fixed during structural optimization to represent the bulk of the material. Figure 7 shows the lowest energy configurations for CH_4 (a) and CO_2 (b) molecules. CH_4 molecule is physisorbed on the surface of the slab near the Co atom and therefore remains unperturbed (see Fig. 7a). The calculated adsorption energy of this molecule is − 0.42 eV. CO_2 molecule is adsorbed more strongly to the surface with adsorption energy of − 0.93 eV. The electronic structure analysis shows the covalent bond formation between the molecule and Co atom of the material (Fig. 7b). Indeed, we obtained a strong overlap of the electron localization function between the molecule and the substrate. Thus, DFT calculations also reveal strong gas adsorption properties of the synthesized $Rb_2Co(H_2P_2O_7)\cdot 2H_2O$ material.

Conclusions

The new pyrophosphate $Rb_2Co(H_2P_2O_7)\cdot 2H_2O$ compound was successfully synthesized in a solution-like and was found to crystallize in the triclinic system, space group ($P\bar{1}$). Its UV–Vis spectrum has shown the usual transitions between the ground state 4T1g and the supper levels 4T2g, 4A2g and 4T1g(P). The sorption results clearly revealed that the prepared compound manifested a high adsorption capacity of the CO_2 and CH_4 gases at different pressures and temperatures. By increasing the temperature, the sorption capacity decreased and increases with respect to the pressure, leading to high sorption values which are quite normal thermodynamically. However, a common adsorption/desorption track of pressure trends alludes to the physisorption phenomena. More interestingly, gas sorption comparison study showed clear evidence of a selective behavior of the acidic pyrophosphate $Rb_2Co(H_2P_2O_7)\cdot 2H_2O$ crystal for CO_2 and CH_4 gases at each temperature and pressure, and revealed also that the sample adsorbtivity of CO_2 is more than that of the CH_4 at different temperatures and pressures. Computer simulations also reveal the selectivity of the material to CO_2 molecules as compared to methane molecules.

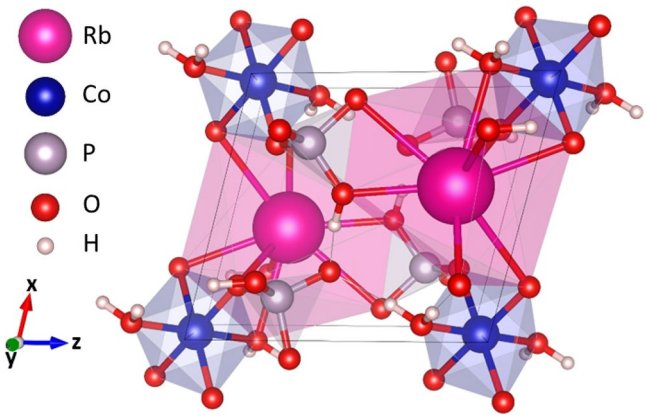

Figure 6. Optimized unit cell structure of $Rb_2Co(H_2P_2O_7)_2\cdot 2H_2O$.

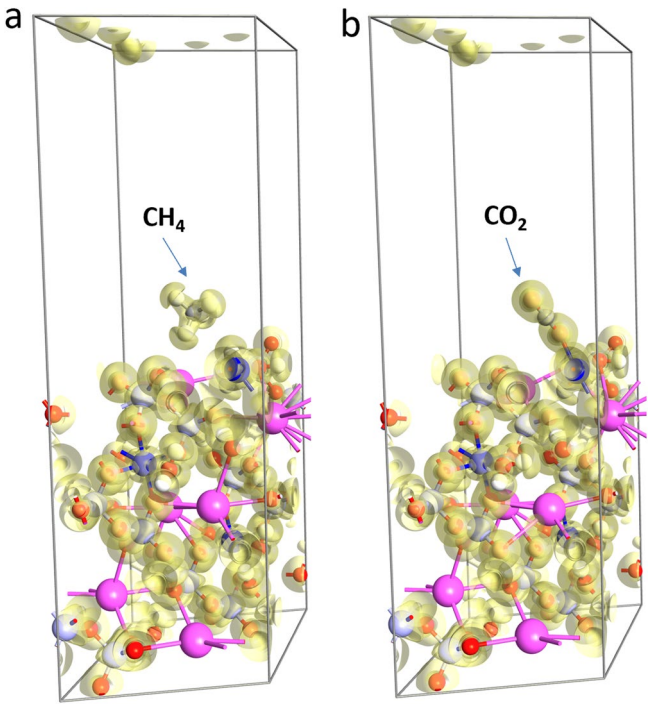

Figure 7. Lowest energy configurations for CH_4 (**a**) and CO_2 (**b**) molecules on Co-terminated 111 surface of $Rb_2Co(H_2P_2O_7)_2{\cdot}2H_2O$. The figure also shows the isosurface plots (isovalue ± 0.1 $Å^{-3}$) of the electron difference density.

Data availability

Supplementary tables of crystal structures and refinements, notably full bond lengths and angles, and anisotropic thermal parameters have been deposited with the Inorganic Crystal Structure Database, FIZ, Hermann von Helmholtz Platz 1, 76344 Eggenstein Leopoldshafen, Germany; fax: (+49) 7247 808 132; Email: crysdata@fiz-karlsruhe.de. CSD-deposition numbers are respectively 421807 for $Rb_2Co(H_2P_2O_7){\cdot}2H_2O$.

Received: 30 November 2022; Accepted: 14 March 2024
Published online: 19 March 2024

References

1. Uma Maheswari, A. & Palanivelu, K. Carbon dioxide capture and utilization by alkanolamines in deep eutectic solvent medium. *Ind. Eng. Chem. Res.* **54**, 11383–11392 (2015).
2. Khalifa, A. A., Ibrahim, A.-J., Amhamed, A. I. & El-Naas, M. H. Accelerating the transition to a circular economy for net-zero emissions by 2050: A systematic review. *Sustainability* **14**, 11656 (2022).
3. Abdullatif, Y. *et al.* Emerging trends in direct air capture of CO_2: A review of technology options targeting net-zero emissions. *RSC Adv.* **13**, 5687–5722 (2023).
4. Abotaleb, A., El-Naas, M. H. & Amhamed, A. Enhancing gas loading and reducing energy consumption in acid gas removal systems: A simulation study based on real NGL plant data. *J. Nat. Gas Sci. Eng.* **55**, 565–574 (2017).
5. Sze, L. L. *et al.* Ternary deep eutectic solvents tasked for carbon dioxide capture. *ACS Sustain. Chem. Eng.* **2**, 2117–2123 (2014).
6. Leron, R. B., Caparanga, A. & Li, M. Carbon dioxide solubility in a deep eutectic solvent based on choline chloride and urea at T = 303.15–343.15 K and moderate pressures. *J. Taiwan Inst. Chem. Eng.* **44**, 879–885 (2013).
7. Lu, M. *et al.* Solubilities of carbon dioxide in the eutectic mixture of levulinic acid (or furfuryl alcohol) and choline chloride. *J. Chem. Thermodyn.* **88**, 72–77 (2015).
8. Lin, C., Leron, R. B., Caparanga, A. R. & Li, M. Henry's constant of carbon dioxide-aqueous deep eutectic solvent (choline chloride/ethylene glycol, choline chloride/glycerol, choline chloride/malonic acid) systems. *J. Chem. Thermodyn.* **68**, 216–220 (2014).
9. Abbott, A. P., Capper, G., Davies, D. L., Rasheed, R. K. & Tambyrajaha, V. Novel solvent properties of choline chloride/urea mixtures. *Chem. Commun.* **7**, 70–71 (2003).
10. Chen, Y. *et al.* Solubilities of carbon dioxide in eutectic mixtures of choline chloride and dihydric alcohols. *J. Chem. Eng. Data* **59**, 1247–1253 (2014).
11. Francisco, M., van den Bruinhorst, A. & Kroon, M. C. Low- transition-temperature mixtures (LTTMs): A new generation of designer solvents. *Angew. Chem. Int. Ed.* **52**, 3074–3085 (2013).
12. Kim, Y. K. *et al.* Crystal-size effects on carbon dioxide capture of a covalently alkylamine-tethered metal-organic framework constructed by a one-step self-assembly. *Sci. Rep.* **6**, 1–8 (2016).
13. Wei, Y. *et al.* Periodic mesoporouso nanocubes with ultrahigh surface areas for efficient CO_2 adsorption. *Sci. Rep.* **6**(6), 1–11 (2016).
14. Guo, T. *et al.* Adsorption characteristics of carbon dioxide gas on a solid acid derivative of β-cyclodextrin. *Energy Fuels* **31**, 4186–4192 (2017).
15. Takamizawa, S. *et al.* Crystal transformation and host molecular motions in CO_2 adsorption process of a metal benzoate pyrazine (MII = Rh, Cu). *J. Am. Chem. Soc.* **132**, 3783–3792 (2010).
16. Joo-Youp, L., Tim, K. C. & Yang, Y. J. Potential flue gas impurities in carbon dioxide streams separated from coal-fired power plants. *J. Air Waste Manag. Assoc.* **59**(6), 725–732 (2009).

17. Chang, Y.-L., Wang, Y.-Z., Ban, D.-M., Yang, B. & Zhao, G.-M. A novel phosphorus-containing polymer as a highly effective flame retardant. *Macromol. Mater. Eng.* **289**, 703–707 (2004).
18. Ali, M. M., El-Hiti, G. A. & Yousif, E. Photostabilizing efficiency of poly(vinyl chloride) in the presence of organotin(IV) complexes as photostabilizers. *Molecules* **21**(1151), 1–16 (2016).
19. Yousif, E., El-Hiti, G. A., Hussain, Z. & Altaie, A. Viscoelastic, spectroscopic and microscopic study of the photo irradiation effect on the stability of PVC in the presence of sulfamethoxazole Schiff's bases. *Polymers* **7**, 2190–2204 (2015).
20. Rozyyev, V. *et al.* High-capacity methane storage in flexible alkane-linked porous aromatic network polymers. *Nat. Energy* **4**, 604–611 (2019).
21. Essehli, R., El Bali, B., Lachkar, M. & Cruciani, G. Two new acidic diphosphates Rb2M(H2P2O7)2·2H2O (M = Zn and Mg): Crystal structures and vibrational study. *J. Alloys Compd.* **492**, 358–362 (2010).
22. Essehli, R. *et al.* K2M (H2P2O7) 2·2H2O (M = Ni, Cu, Zn): Orthorhombic forms and Raman spectra. *Acta Cryst. Sect.* **C61**, i120–i124 (2005).
23. Essehli, R., El Bali, B., Lachkar, M. & Michael, B. Dicaesium magnesium bis(dihydrogen phosphate(V) dihydrate. *Acta Cryst. Sect.* **E65**, i3–i3 (2009).
24. Essehli, R., Lachkar, M., Svoboda, I., Fuess, H. & El Bali, B. (NH4)2[Ni(H2P2O7)2(H2O)2]. *Acta Cryst. Sect.* **E61**, i64–i66 (2005).
25. Essehli, R., Lachkar, M., Svoboda, I., Fuess, H. & El Bali, B. (NH4)2[Co(H2P2O7)2(H2O)2]. *Acta Cryst. Sect.* **E61**, i61–i63 (2005).
26. Essehli, R., Lachkar, M., Svoboda, I., Fuess, H. & El Bali, B. Synthesis, crystal structure and vibrational spectra of a new diammonium zinc (II) dihydrogendiphosphate dihydrate, (NH4)2 Zn (H2P2O7) 2· 2H2O. *Acta Cryst. Sect.* **E61**, i32–i34 (2005).
27. Clark, R. C. & Reid, J. S. *CrysAlis RED, Oxford Diffraction Ltd., Program for analytical numeric absorption correction, Version 170*, 17 (2003).
28. Sheldrick, G. M. *SHELXS-97, Program for the Solution of Crystal Structures* (University of Göttingen, 1990).
29. Sheldrick, G. M. *SHELXL-97, Program for Crystal Structure Determination* (University of Göttingen, 1997).
30. Brandenburg, K. *DIAMOND, Crystal Impact GbR, Bonn, Germany, Version 2.1 e* (2001).
31. Zulfiqar, S. *et al.* Amidoxime porous polymers for CO_2 capture. *RSC Adv.* **3**, 17203–17213 (2013).
32. Cristancho, D. E. *et al.* Force transmission error analysis for a high-pressure single-sinker magnetic suspension densimeter. *Int. J. Thermophys.* **31**, 698–709 (2010).
33. Altamash, T. *et al.* Carbon dioxide solubility in phosphonium-, ammonium-, sulfonyl-, and pyrrolidinium-based ionic liquids and their mixtures at moderate pressures up to 10 bar. *J. Chem. Eng. Data* **62**, 1310–1317 (2017).
34. Perdew, J. P., Burke, K. & Ernzerhof, M. Generalized gradient approximation made simple. *Phys. Rev. Lett.* **77**, 3865 (1996).
35. Monkhorst, H. K. & Pack, J. D. Special points for Brillouin-zone integrations. *Phys. Rev. B* **13**, 5188 (1976).
36. Becke, A. D. & Edgecombe, K. E. A simple measure of electron localization in atomic and molecular systems. *J. Chem. Phys.* **92**, 5397–5403 (1990).
37. Smidstrup, S. *et al.* First-principles Green's-function method for surface calculations: A pseudopotential localized basis set approach. *Phys. Rev. B* **96**, 195309 (2017).
38. Smidstrup, S. *et al.* QuantumATK: An integrated platform of electronic and atomic-scale modelling tools. *J. Phys.: Condens. Matter* **32**, 015901 (2020).
39. Altamash, T., Amhamed, A. I., Aparicio, S. & Atilhan, M. Combined experimental and theoretical study on high pressure methane solubility in natural deep eutectic solvents. *Ind. Eng. Chem. Res.* **58**, 8097–8111 (2019).
40. Essehli, R. *et al.* Single crystal structure, vibrational spectroscopy, gas sorption and antimicrobial properties of a new inorganic acidic diphosphates material (NH4)2Mg(H2P2O7)2·2H2O. *Sci. Rep.* **10**, 1–10 (2020).
41. Abotaleb, A., El-Naas, M. H. & Amhamed, A. Enhancing gas loading and reducing energy consumption in acid gas removal systems: A simulation study based on real NGL plant data. *J. Nat. Gas Sci. Eng.* **S1875–5100**, 30346–30353 (2017).
42. Atilhan, M., Altamash, T. & Aparicio, S. Quantum chemistry insight into the interactions between deep eutectic solvents and SO_2. *Molecules* **24**, 1–18 (2019).
43. Altamash, T. *et al.* Rheological, thermodynamic, and gas solubility properties of phenylacetic acid-based deep eutectic solvents. *Chem. Eng. Technol.* **40**, 778–790 (2017).
44. Amhamed, A., Atilhan, M. & Berdiyorov, G. Permeabilities of CO_2, H2S and CH4 through choline-based ionic liquids: Atomistic-scale simulations. *Molecules* **27**(27), 24 (2019).
45. Karadas, F. *et al.* CO_2 adsorption studies on hydroxy metal carbonates $M(CO_3)x(OH)y$ (M = Zn, ZnMg, Mg, MgCu, Cu, Ni, and Pb) at high pressures up to 175 bar. *Langmuir* **27**, 10642–10647 (2011).
46. Tian, X. *et al.* A DFT based method for calculating the surface energies of asymmetric MoP facets. *Appl. Surf. Sci.* **427**, 357–362 (2018).
47. Onawole, A. T., Hussein, I. A., Carchini, G., Sakhaee-Pour, A. & Berdiyorov, G. R. Effect of surface morphology on methane interaction with calcite: A DFT study. *RSC Adv.* **10**, 16669 (2020).

Acknowledgements

Authors acknowledge the financial and technical support from Qatar Environment and Energy Research Institute (QEERI), Hamad Bin Khalifa University, Qatar Foundation. Part of this research was conducted at Oak Ridge National Laboratory (ORNL), managed by UT Battelle, LLC, for the U.S. Department of Energy (DOE) under contract DE-AC05-00OR22725. Authors acknowledge the financial support from Qatar Environment and Energy Research institute (QEERI), Hamad bin Khalifa University (HBKU) (member of Qatar Foundation) and Qatar National Research Fund, Grant# NPRP12C-0821-190017, Doha, Qatar. R. Essehli and B. El Bali would also to thank I. Svoboda and H. Fuess (Technische Universität Darmstadt, Petersenstrasse 23, 64287 Darmstadt, Deutschland) for the crystal structure investigations.

Author contributions

R.E. designed the crystal structure, synthesis, characterization, initial draft of material part. A.A. design the experimental of CO2 and CH4 adsorption and storage measurement, review the process concept and edited the final manuscript. B.A. supported the materials characterization and writing the manuscript. T.A. conducted the experimental measurement for CO2 and CH4, and draft the writing of experimental part. M.A., B.E. and M.L. reviewed the characterization and experimental parts. G.R.B. conducted the simulation calculation and participated in manuscript writing up. All authors contributed to manuscript preparation and reviewing processes. A.A. directed the project.

Competing interests

The authors declare no competing interests.

Additional information

Supplementary Information The online version contains supplementary material available at https://doi.org/10.1038/s41598-024-57060-8.

Correspondence and requests for materials should be addressed to A.A.

Reprints and permissions information is available at www.nature.com/reprints.

Publisher's note Springer Nature remains neutral with regard to jurisdictional claims in published maps and institutional affiliations.